The Real-Time Monitoring of the Thermal Unfolding of Tetramethylrhodamine-Labeled Actin[†]

Alexandru A. Perieteanu and John F. Dawson*

Department of Molecular and Cellular Biology, University of Guelph, Guelph, Ontario, Canada N1G 2W1

Received March 11, 2008; Revised Manuscript Received May 28, 2008

ABSTRACT: Modification of actin at Cys^{374} with tetramethylrhodamine maleimide (TMR-actin) has been used for visualization of actin filaments and to produce high-resolution crystal structures of actin. We show that TMR-actin exhibits a 21% decrease in absorbance at 557 nm upon thermal unfolding, likely due to the movement of TMR to a more hydrophobic environment upon rapid unfolding and protein aggregation. We took advantage of this property to test models of actin protein unfolding. A transition temperature (T_m) of 60.2 ± 0.2 °C for Ca^{2+}•ATP•TMR-actin was determined using A_{557} and agreed with our own determinations employing different techniques and previous work with unlabeled actin. Our data show that the dependence of TMR-actin thermal stability on the bound nucleotide and cations follows a trend of Ca^{2+}•ATP > Mg^{2+}•ATP > Ca^{2+}•ADP > Mg^{2+}•ADP. The activation energies and frequency factors for the thermal unfolding of TMR-actin determined with two methods were in good agreement with those previously determined for unlabeled actin. We observed a biphasic trend in the T_m of TMR-actin with increasing nucleotide concentrations, supporting a two-pathway model for actin protein unfolding where one pathway dominates at different concentrations of nucleotide. Additionally, TMR-actin bound by DNase I or gelsolin segment-1 exhibited elevated transition temperatures.

Actin is a 42 kDa protein that is a major component of the eukaryotic cytoskeleton. Actin is intimately involved in many physiological processes, including organelle trafficking and muscle contraction (*1, 2*). Variants of actin with reduced stability may be related to the development of diseases (*3*). A common measure of the stability of proteins is the transition temperature, also known as the melting temperature (T_m).[1] Determining the T_m and unfolding pathways of actin proteins may therefore provide insight into the molecular mechanism of some diseases.

Under physiological conditions, actin is stabilized by a nucleotide and divalent cation bound between the two major domains, preventing the domains from rotating with respect to one another (*4*). Although nucleotide-free actin is still functional, 30% sucrose is required to maintain its stability (*5*). In the absence of sucrose, nucleotide-free actin quickly unfolds and becomes inactive. The nucleotide binding affinity of actin is greatly increased when divalent cation is bound (*6*). In its most stable form, a cation coordinated nucleotide can be found within the nucleotide binding cleft of actin (MNA), where M represents the cation (metal), N represents the nucleotide, and A represents actin. It is believed that the loss of both metal and cation are prerequisites for the unfolding of actin (*7–9*). Two major pathways are thought to dominate the kinetic mechanism for metal and nucleotide loss in actin: (1) the dissociation of cation leads to a nucleotide bound actin (NA) intermediate where actin's affinity for nucleotides is greatly reduced and the nucleotide is quickly released, forming an unbound actin intermediate (A), and (2) the dissociation of the cation and nucleotide occurs simultaneously as a complex (MN) leading to the unbound actin intermediate. Subsequently, the unbound actin intermediate quickly unfolds, losing ~30% of its helical content and forming an essentially unfolded actin intermediate (U*). Studies have shown that, in the absence of protein

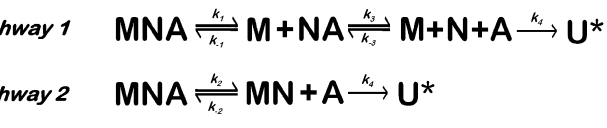

denaturants, the essentially unfolded actin intermediate has a tendency to form large monodispersed actin associates of approximately 15 times the molecular weight of actin (inactivated actin, I_{15}) (*10*). In the presence of denaturants, essentially unfolded actin completely unfolds, losing the majority of its secondary structural characteristics (*10*). The unfolding of actin *via* GdnHCl, EDTA, and thermal exposure is thought to be an irreversible process, reversible only under nonaggregating conditions in the presence of molecular chaperonin CCT (*8*). A model for the complete unfolding of actin is described in pathway 3 (for a current review see ref *9*).

The thermal stability of actin has been studied using differential scanning calorimetry (*11*), circular dichroism

[†] This research was supported by the Natural Sciences and Engineering Research Council of Canada, Grant 250188-04 to J.F.D.

* To whom correspondence should be sent. Tel: (519) 824-4120 ext 58181. Fax: (519) 837-1802. E-mail: jdawso01@uoguelph.ca.

[1] Abbreviations: T_m, transition temperature; TMR, tetramethylrhodamine maleimide; M•N•TMR-actin, describes the metal and nucleotides bound to the actin species; DTT, dithiothreitol; GS1, human gelsolin segment-1; DNase I, bovine pancreas deoxyribonuclease I; DMF, dimethylformamide; $A_{\#}$, wavelength of absorbance measurements; λ_{max}, wavelength of maximum absorbance; NAc, *N*-acetyl; DSC, differential scanning calorimetry; CD, circular dichroism.

10.1021/bi800421u CCC: $40.75
Published on Web 08/15/2008

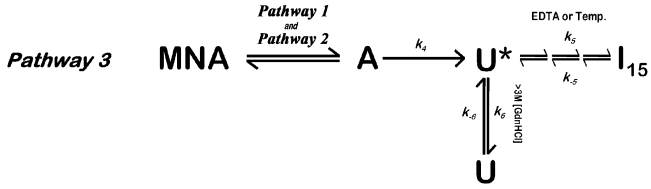

(*12*), and tryptophan phosphorescence, each requiring significant quantities of protein and specialized equipment. To circumvent these limitations, Schuler et al. used a DNase I inhibition assay to indirectly report on the folding state of actin (*7*). Using the methods mentioned, a variety of melting temperatures for Ca^{2+}•ATP muscle actin, ranging from 57.2 to 64.6 °C, have been reported (Table 1) (*7, 11, 13*−*17*).

Actin can be covalently modified at Cys^{374} by tetramethylrhodamine-5-maleimide (TMR). The impact of TMR modification on the function of actin has been well characterized (*15, 18–20*). Gel filtration of TMR-actin labeling reactions yielded two specific elution species: a species eluting at the void volume of the column with a redish-purple color and a species corresponding to the molecular mass of actin monomer with a pink hue. Both eluates were shown (*via* SDS−PAGE) to contain only actin. We hypothesized that the large molecular mass eluate was inactivated actin aggregate and that the absorbance of TMR-actin changes from a folded to an inactivated state. The objectives of this paper were (1) to test the hypothesis that TMR-actin undergoes a change in absorbance upon inactivation, (2) to determine whether a change in TMR-actin absorbance could be used as a convenient and valid method for studying actin stability in comparison to other work, (3) to contribute to the current understanding of actin unfolding models with respect to nucleotides and cations, and (4) to extend this method to study actin-containing protein complexes.

In this work, we demonstrate that monitoring the change in absorbance of TMR-actin provides a robust and accurate technique for the measurement of actin stability. We have extended this technique to studies with different nucleotides and cations thus contributing to the understanding of a thermal unfolding pathway dominated by two kinetic pathways. Additionally, we have found that monomeric actin is stabilized by the binding of deoxyribonuclease I (DNase I) or gelsolin segment-1 (GS1).

EXPERIMENTAL PROCEDURES

Reagents. All reagents used were purchased from Sigma-Aldrich (St. Louis, MO) with the exception of tetramethylrhodamine-5-maleimide, which was purchased from Invitrogen (Burlington, ON) or AnaSpec (San Jose, CA) and molecular grade ATP (Fisher Scientific, Mississauga, ON). A Super-Q Millipore filtration system was used to purify all of the water used to a resistivity of 18 MΩ. All chromatographic columns, including Sephadex resin, were supplied by GE Healthcare (Piscataway, NJ).

Protein Preparation. Actin from chicken muscle acetone powder was prepared as described (*21*). Actin concentrations were determined from absorbance at 290 nm using an extinction coefficient of 67742 M^{-1} cm^{-1} or using the Bio-Rad Protein Assay (Hercules, CA). Actin samples were frozen in N_2(l) and stored at −80 °C.

Chicken actin was labeled at Cys^{374} with TMR. G-actin (2−10 mL, 1−5 mg/mL) was treated with a 10-fold molar excess of dithiothreitol (DTT) and incubated at 4 °C for 2 h to reactivate SH groups. HiTrap desalting columns were then used to remove DTT. A 2-fold molar excess of TMR in dimethylformamide (DMF) was added to G-actin and incubated overnight at 4 °C under low light conditions. The labeling reaction was quenched using a 2-fold molar excess of DTT. Excess TMR was then separated from TMR-actin employing a 20 mL Sephadex G-25 column equilibrated in G-buffer or HiTrap desalting columns. Two successive polymerization and depolymerization cycles were then performed to remove unlabeled actin. Polymerization conditions were achieved using a 10× concentrated stock of salts to a final composition of 25 mM TrisHCl, pH 8.0, 50 mM KCl, 1.0 mM EGTA, 2.0 mM $MgCl_2$, and 0.1 mM ATP. Polymerized actin and large protein aggregates were then removed by centrifugation at 490000*g* for 20 min at 4 °C. Further purification of TMR-actin was performed using a Sephacryl S-300 26/60 column equilibrated in G-buffer (2 mM TrisHCl, pH 8.0, 0.2 mM $CaCl_2$, 0.2 mM ATP, 0.2 mM β-mercaptoethanol). TMR labeling efficiency was found to be >95% by MALDI-TOF spectrometry. Unless otherwise stated, TMR-actin samples were stored in nonreducing G-buffer under low light conditions at 4 °C and used within one week of purification.

To acquire Ca^{2+}•ADP•TMR-actin, freshly prepared Ca^{2+}•ATP•TMR-actin was buffer exchanged into G-buffer in which 0.2 mM ADP was substituted for ATP. The sample was incubated with 20 U/mL hexokinase in the presence of 0.3 mM glucose for 16 h and subsequently buffer exchanged into G-buffer containing ADP. Cation exchange for the formation of Mg^{2+}•ATP•TMR-actin was accomplished by incubation with 0.5 mM EGTA and 2 mM $MgCl_2$ for 15 min followed by buffer exchange into 0.2 mM $MgCl_2$, 0.2 mM ATP, 2 mM TrisHCl, pH 8.0. Mg^{2+}•ADP•TMR-actin was formed by nucleotide exchange followed by cation exchange as described above.

Human gelsolin segment-1 was prepared as described (*22*) and stored at −80 °C. Prior to use, GS1 was thawed and exchanged into G-buffer using HiTrap desalting columns. GS1 concentrations were determined using Bio-Rad protein assay. Bovine pancreas deoxyribonuclease I stabilized in glycine was purchased from Worthington Biochemical Corp. (Lakewood, NJ).

TMR-Actin Complex Formations. A 1.5−2 molar excess of GS1 was added to TMR-actin and incubated at room temperature for 20 min. The mixture was then applied to a MonoQ 5/5 column and eluted with an increasing 0.5 M KCl gradient. GS1-bound TMR-actin-containing fractions were identified by SDS−PAGE, pooled, and buffer exchange into G-buffer was performed.

DNase I-bound TMR-actin was formed by combining a 1.5−2 molar excess of DNase I with TMR-actin and incubating at 4 °C for 2 h. The heterodimer was purified using a Superdex S-200 26/60 gel filtration column equilibrated in G-buffer containing 50 mM NaCl. Buffer exchange into G-buffer was performed on the DNase I-bound TMR-actin complex-containing fractions and concentrated using Millipore (Billerica, MA) concentrators. All complexes were used within 1 week of their purification. Native PAGE showed no unbound TMR-actin present in the GS1 or DNase I heterodimer samples.

Table 1: Summary of the Previously Reported Thermal Transition Temperatures for Skeletal Actin

isoform	method	buffer	scan rate (°C/min)	T_m (°C)	E_a (kJ/mol)	ref
rabbit skeletal	DSC	0.2 mM ATP, 0.2 mM $CaCl_2$, 2 mM HEPES, pH 8.0	0.5	57.2 ± 0.5		*13*
rabbit skeletal	DSC	0.1 mM ATP, 0.5 mM $CaCl_2$, 2 mM TrisHCl, pH 7.6	0.63	60.8	231 ± 17,[a] 285 ± 2	*11*
rabbit skeletal	DNase I	0.2 mM ATP, 0.2 mM $CaCl_2$, 2 mM TrisHCl, pH 8.0	0.67	60.4 ± 0.3	269 ± 31,[a] 291 ± 25[b]	*7*
rabbit skeletal	fluorescence	0.2 mM ATP, 0.2 mM $CaCl_2$, 2 mM HEPES, pH 7.6	0.7	56.7		*13*
rabbit skeletal	DSC	0.2 mM ATP, 0.2 mM $CaCl_2$, 2 mM TrisHCl, pH 8.0	1.0	60.3		*17*
chicken skeletal	DNase I	0.2 mM ATP, 0.25 mM $CaCl_2$, 5 mM TrisHCl; pH 8.26	1.0	~60		*14*
TMR-rabbit skeletal	DSC	0.2 mM ATP, 0.2 mM $CaCl_2$, 2 mM TrisHCl, pH 8	1.0	64.6 ± 0.9		*15*
TMR-rabbit skeletal	DSC	0.2 mM ATP, 0.2 mM $CaCl_2$, 2 mM TrisHCl, pH 8	1.0	64.0 ± 0.7		*15*
chicken skeletal	DSC	0.2 mM ATP, 0.2 mM $CaCl_2$, 2 mM TrisHCl, pH 8.26	1.0	64.3−64.5		*16*
TMR-chicken skeletal	absorbance	0.2 mM ATP, 0.2 mM $CaCl_2$, 2 mM TrisHCl, pH 8	1.0	63.0 ± 0.1	283 ± 24,[a] 232 ± 20[b]	current study
TMR-chicken skeletal	absorbance	0.2 mM ATP, 0.2 mM $CaCl_2$, 2 mM TrisHCl, pH 8	0.5	60.2 ± 0.2		current study

[a] E_a determined from the kinetics of unfolding. [b] E_a determined from the T_m dependence on the scan rate.

T_m Analysis via Absorbance Measurements. All absorbance measurements were taken using a Beckman DU800 spectrophotometer (Mississauga, ON) equipped with a high-performance Peltier temperature control unit. Accuracy of the Peltier unit was verified at variable scan rates. The temperature was increased from 25 to 85 °C at a rate of 0.5 °C/min unless otherwise stated. Unless otherwise stated, unfolding experiments were carried out on samples containing 10 μM TMR-actin in nonreducing G-buffer. The rates of unfolding were plotted as a function of temperature and a Weibull fit was applied using SigmaPlot 10, Systat Software (Point Richmond, CA). The T_m was considered to be the point at which the rate of protein unfolding was the greatest.

Unfolding Kinetics. The absorbance at 557 nm was normalized to unity representing the fraction of native (N) actin at various times. N at constant temperature was plotted as a function of time and fit to $N = Ae^{-k_{app}t}$. The k_{app} determined at various temperatures was then plotted as a function temperature, and the activation energies for the unfolding of TMR-actin, GS1-bound TMR-actin, and DNase I-bound TMR-actin were determined from the slope of the curves dictated by the Arrhenius equation, $k_{app} = Ae^{E_a/RT}$.

RESULTS

Monitoring TMR Absorbance as an Assay for Actin Thermal Unfolding. When tetramethylrhodamine was bound to Cys^{374} at the C-terminal end of skeletal α-actin, a distinct absorbance profile based on the folding state of the protein was observed (Figure 1A). Folded TMR-actin showed an absorbance maximum at 557 nm with a shoulder at 522 nm. After 30 min exposure at 75 °C, a 5 nm blue shift in the absorbance maximum from 557 to 552 nm was observed. The absorbance magnitudes at 557 and 552 nm decreased by 21% and 11%, respectively. Monitoring the absorbance change at 557 nm yielded a sigmoidal decrease in the absorbance with increasing temperature (Figure 1B). The rate at which the absorbance changed with temperature followed a trend resembling an asymmetric parabolic curve with minima corresponding to the temperature at which the rate of TMR-actin unfolding was at a maximum (transition temperature). A Weibull fit was applied to the curve to extrapolate an unbiased minimum (Figure 1C).

The change in TMR-actin absorbance upon unfolding likely reflects a different environment experienced by the TMR moiety. To determine if the TMR on actin enters a more or less polar environment upon unfolding, we monitored the absorbance of NAc-Cys-TMR at 557 nm at different dielectric constants (ϵ) (Figure 1D). We found that the dependence of A_{557} of NAc-Cys-TMR on ϵ was biphasic. At ϵ values below 27, the A_{557} increased at a linear rate of +5.6% A_{557}/ϵ, while above an ϵ value of 27, the A_{557} decreased at a linear rate of −0.2% A_{557}/ϵ. Based on these data, a 21% change in the A_{557} of TMR, as seen with TMR-actin, can only reasonably occur by movement of the TMR moiety to a low ϵ, apolar environment. A blue shift in the λ_{max} of NAc-Cys-TMR was also observed as ϵ decreased below 27, consistent with the blue shift in λ_{max} of TMR-actin seen upon thermal unfolding of actin.

By monitoring absorbance at 557 nm, we observed a transition temperature of 60.2 ± 0.2 °C for Ca^{2+}•ATP•TMR-actin. As an internal control, our values were found to compare favorably with our respective T_m values of 62.5 ± 0.2 °C and 61.8 ± 0.1 °C for Ca^{2+}•ATP•TMR-actin employing DNase I inhibition and the weak change in A_{304} (Figure 2). The change in A_{304} was previously hypothesized to be a result of the movement of tryptophan residues away from positively charged side chains upon the temperature-induced unfolding of actin (*12*). Our values also compare favorably with previously reported values of 60.4 ± 0.3 °C using DNase I inhibition and 60.3 °C using DSC (Table 1) (*7, 17*).

Actin Unfolding as an Irreversible Two-State Process. TMR-actin samples that underwent thermal unfolding and were cooled did not exhibit a decrease in A_{557} upon a second thermal gradient treatment, confirming that the actin unfold-

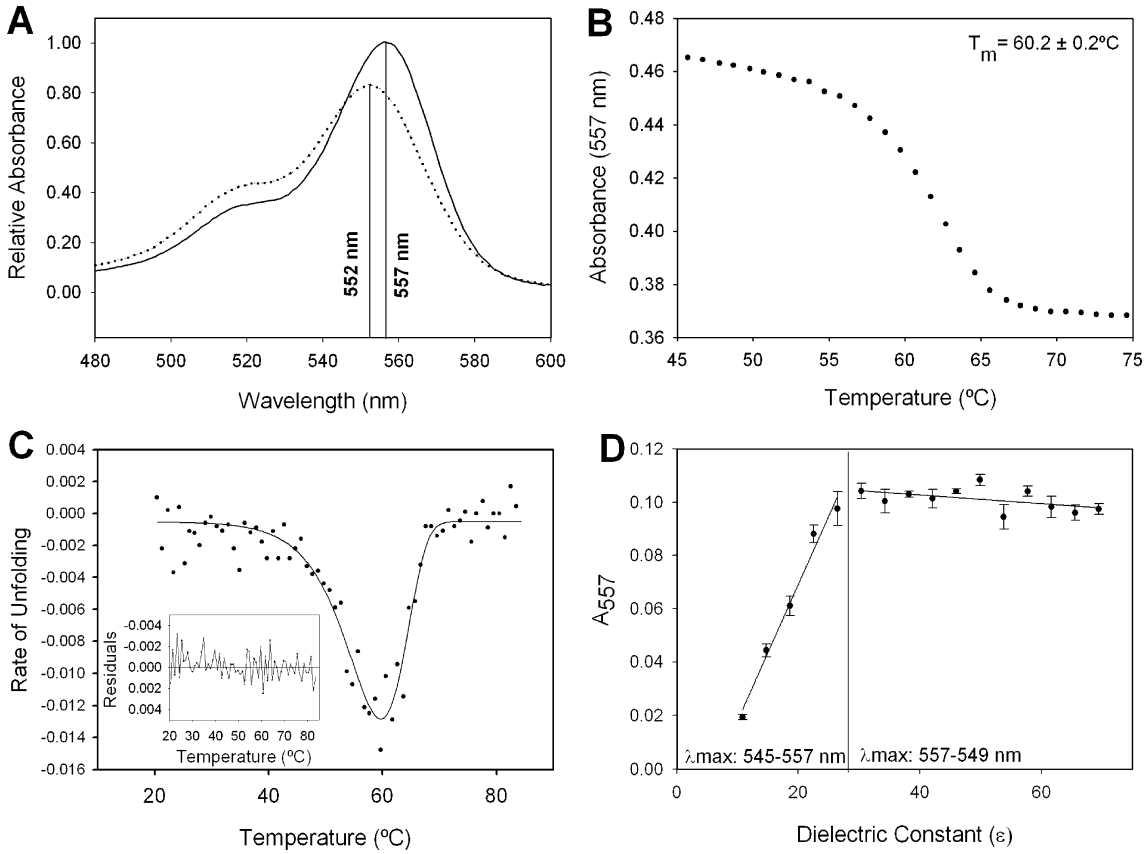

FIGURE 1: Monitoring the absorbance at 557 nm allows for the determination of the T_m of actin. (A) Wavelength scan of 10 μM folded TMR-actin (solid line) and 10 μM TMR-actin incubated at 75 °C for 30 min (dotted line). A 5 nm blue shift in λ_{max} and 21% decrease in A_{557} of TMR-actin are observed upon thermal denaturation. (B) Typical data acquired for 10 μM Ca^{2+}•ATP•TMR-actin by monitoring A_{557} through a thermal gradient of 0.5 °C/min. (C) The rate of the absorbance change with respect to temperature ($\Delta A_{557}/\Delta T$) from panel B was plotted as a function of temperature. To generate unbiased values, a Weibull fit was applied and the temperature corresponding to the absolute maximum $\Delta A_{557}/\Delta T$ taken to be the T_m. A residual plot (inset) shows a good fit with no trends in deviation. Weibull fits were used for every T_m determination conducted employing A_{557}. A melting temperature of 60.2 ± 0.2 °C ($n = 12$) was determined for Ca^{2+}•ATP•TMR-actin. (D) A_{557} measurements of 2 μM NAc-Cys-TMR at various polarities created by ratios of 1,4-dioxane (ϵ of 2.2) and 18 MΩ water (ϵ of 80.3 at 20 °C) (v/v). Two linear regions of A_{557} change were found: at ϵ lower than 27, the $\Delta A_{557}/\Delta\epsilon$ was an increase of 5.6% A_{557}/ϵ, while above an ϵ of 27, a decrease of −0.2% A_{557}/ϵ was observed. The ranges of λ_{max} in each region of the curve are listed at the bottom of the graph. A linear increase in λ_{max} from 545 to 557 nm at lower ϵ was observed with a λ_{max}/ϵ of 0.64 nm/ϵ. Beyond ϵ of 27, linearity was lost, and the λ_{max} decreased from 557 to 549 nm at ϵ of 70. Error bars represent standard error.

ing reaction is irreversible under the conditions tested (data not shown). We have shown that the change in A_{557} is due to the transformation from folded actin to an actin aggregate, perhaps like that of the I_{15} species described earlier (*10*). Pathway 3 can be simplified to a two-state irreversible process such that MNA → I_{15}, if I_{15} is thermally stable and rapidly achieved from U* and if nucleotide free actin unfolds rapidly. Under these conditions, the Sanchez-Ruiz rule for irreversible kinetic unfolding applies (*23*) in which the T_m of first-order kinetic unfolding varies with the rate of temperature increase (υ, Figure 3) according to the equation:

$$\frac{\upsilon}{T_m^2} = \frac{AR}{E_a} e^{-(E_a/RT_m)} \quad (1)$$

A plot of $\ln(\upsilon/T_m^2)$ versus $1/T_m$ yielded a linear relation with a slope equivalent to an E_a of 232 ± 20 kJ/mol and a frequency factor $\ln(A) = 72$ for Ca^{2+}•ATP-TMR-actin (Figure 3A, inset). These values are in agreement with previously determined values (Table 1). T_m values were experimentally determined at $\upsilon = 0.5$ °C/min and 1.0 °C/min and calculated for $\upsilon = 0.66$ °C/min to compare our data to previously determined values. The values for the unfolding of TMR-actin at 0.5, 0.66, and 1.0 °C/min were 60.2 °C ± 0.2 °C, 61.7 °C, and 63.0 ± 0.1 °C respectively, corresponding with previously reported experimental T_m values at each value of υ (Table 1).

The rate of TMR-actin unfolding at various temperatures can also be used in combination with the Arrhenius equation to determine the activation energy independent of scan rate (Figure 3B). Using the Arrhenius equation, an activation energy of 283 ± 24 kJ/mol and a frequency factor of $\ln(A) = 99$ was determined. In agreement with previous studies by Le Bihan et al. (*11*), raw absorbance measurements at different temperatures yielded similar final absorbance intensities, suggesting that the same amount of inactivated actin is present regardless of the temperature. This observation also supports the irreversibility of the actin unfolding reaction.

Nucleotide and Cation Effects on Actin Stability. We examined the influence of different cations and nucleotides on the T_m of TMR-actin as reported by A_{557} (Figure 4). Our results reflect the trends observed for actin using other methods (*7*). The stabilizing effect of nucleotides and cations was shown to follow a trend of Ca^{2+}•ATP > Mg^{2+}•ATP > Ca^{2+}•ADP > Mg^{2+}•ADP, where ATP-coordinated calcium bound to actin showed the highest thermal stability.

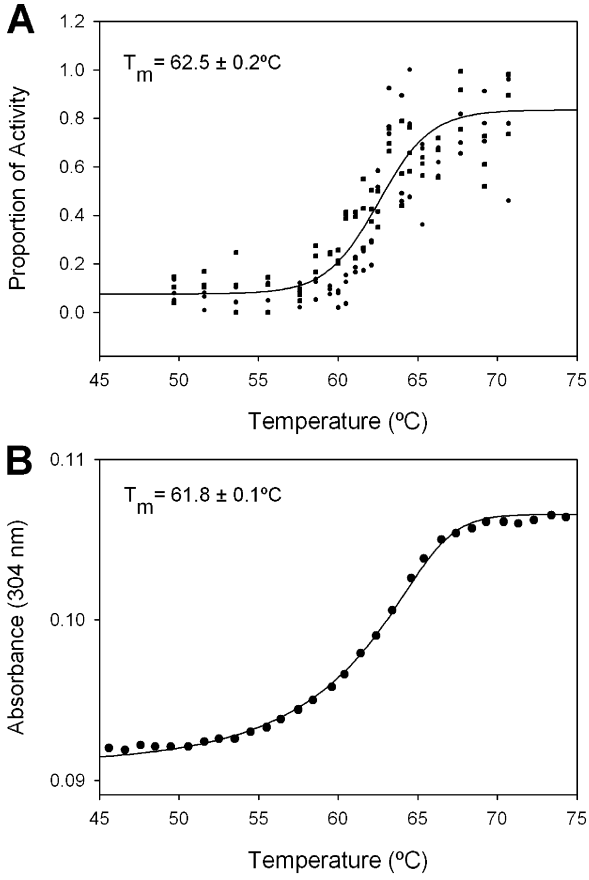

FIGURE 2: The melting temperature of 10 μM Ca^{2+}•ATP-TMR-actin measured with absorbance at 557 nm is similar to that determined by other methods. (A) The melting temperature (T_m) of TMR-actin was determined employing a DNase I inhibition assay to be 62.5 ± 0.2 °C. The data points shown are averages of separate duplicate or triplicate assays with a calculated sigmoidal best fit shown. (B) Absorbance at 304 nm yielded a T_m of 61.8 ± 0.1 °C for TMR-actin (n = 3). Similar to (A), a sigmoidal curve fit was applied using SigmaPlot 10. Note that the magnitude of the change in A_{557} was much greater than that seen at A_{304} and that only about 50% of the A_{304} results yielded usable data.

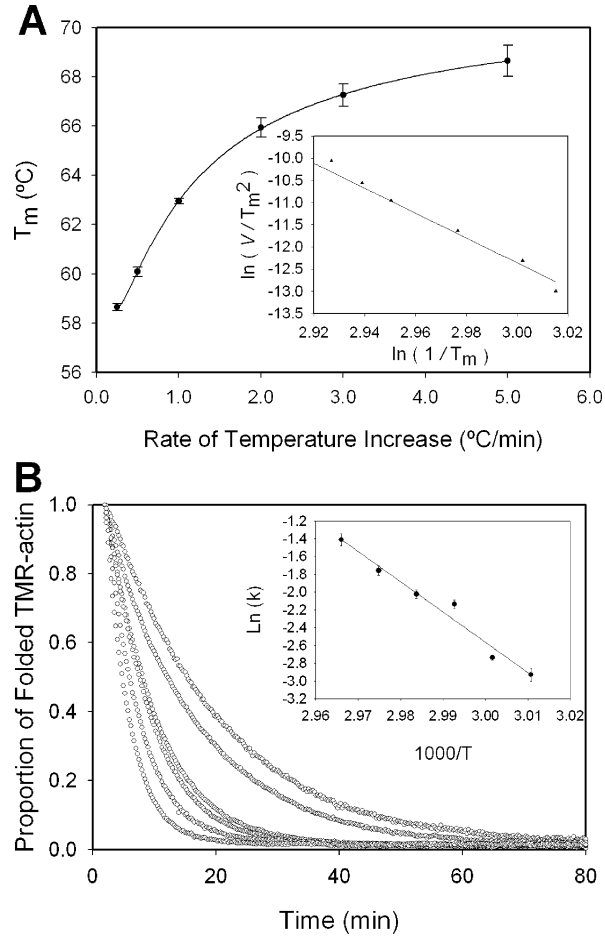

FIGURE 3: Activation energy determinations, through scan rate dependent thermal denaturation, and constant temperature kinetic analysis. (A) The melting temperature of 10 μM Ca^{2+}•ATP•TMR-actin was determined at six different heating rates: 0.25, 0.5, 1.0, 2.0, 3.0, and 5.0 °C/min with n of 5, 12, 5, 5, 5, and 5, respectively. Error bars represent the standard error calculated at the respective heating rates. Using eq 1, the activation energy was determined from the slope of the linearized curve (inset). An activation energy of 232 ± 20 kJ/mol and a frequency factor of 72 ± 7 was calculated. (B) Ca^{2+}•ATP•TMR-actin (10 μM) was subjected to temperatures 59, 60, 61, 62, 63, and 64 °C (right to left). Raw absorbance measurements were normalized to unity, and rates of signal decay were fit to single exponential decay curves using SigmaPlot 10. The natural log of the rates and their respective 1000/T, in units of kelvin, were plotted (inset) and the activation energy derived from the slope of the linear fit in accordance with the Arrhenius equation. The calculated E_a for Ca^{2+}•ATP•TMR-actin was 282 ± 25 kJ/mol with a frequency factor of 99 ± 9. All kinetic parameters were determined from data sets with $n \geq 3$ with error bars representing standard error.

According to actin protein unfolding pathways 1 and 2, the association of nucleotide governs the stability of actin. To test the effects of ATP concentration on the thermal stability of actin, we measured the T_m of Ca^{2+}•ATP-TMR-actin with our A_{557} assay at increasing ATP concentrations while holding the calcium concentration constant at 0.2 mM (Figure 5A). This concentration of calcium was chosen because it is present in commonly employed buffers maintaining actin in the monomeric state. Under these conditions, the T_m of Ca^{2+}•ATP•TMR-actin increased with higher ATP concentrations to a maximum T_m of 61.1 ± 0.1 °C when ATP was 0.1 mM. Above 0.1 mM ATP, the T_m of TMR-actin decreased significantly to 57.9 ± 0.1 °C at an ATP concentration of 1 mM.

Our results show that high ATP concentrations have a negative effect on actin stability. This phenomenon seems contradictory to the hypothesis that the unfolding of actin is rate limited by the loss of bound nucleotide; however, the ability of ATP to chelate divalent cations must be taken into account. A chelation effect would result in the lowering of the concentration of free Ca^{2+} in solution and an increase in the concentration of coordinated Ca^{2+}•ATP, thus increasing the flux of nucleotide loss through pathway 1. To test this hypothesis, we increased the concentrations of calcium and ATP in equimolar amounts. The T_m of TMR-actin increased with increasing amounts of ATP and calcium (Figure 5B). A pseudo-first-order kinetic fit was applied, and a theoretical T_m maximum of 72.7 °C was calculated. To exclude the possibility that increasing ATP concentrations may have a physical effect on the solution properties, the pH of the samples was monitored and found to be stable (Figure 5, inset).

Interaction with Actin Binding Proteins Increases Actin Stability. Studying thermal unfolding using the change in TMR absorbance properties is advantageous because the unfolding of the majority of proteins does not produce a

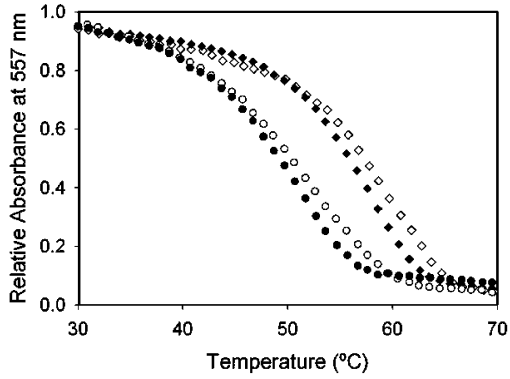

Nucleotide	Cation	$T_m \pm$ SE (ºC)
◇ ATP	Ca^{2+}	60.2 ± 0.2
◆ ATP	Mg^{2+}	55.9 ± 0.8
○ ADP	Ca^{2+}	52.0 ± 0.1
● ADP	Mg^{2+}	50.2 ± 0.3

FIGURE 4: The T_m of TMR-actin (10 μM) differs under various nucleotide and cation conditions. Ca^{2+}•ATP-TMR-actin (open diamonds) was found to have a T_m of 60.1 ± 0.2 °C (n = 12). Ca^{2+}•ADP-TMR-actin (open circles) yielded T_m = 52.0 ± 0.1 °C (n = 5). The Mg^{2+}•ATP-TMR-actin (closed diamonds) and Mg^{2+}•ADP-TMR-actin (closed circles) showed lower T_m values of 55.9 ± 0.8 °C and 50.2 ± 0.3 °C (n = 4 and 4).

signal change in the 557 nm range; therefore, spectral results are not complicated by the presence of other proteins. We have taken advantage of this property to determine the thermal stability of TMR-actin in complex with DNase I and gelsolin segment-1. Actin with DNase I bound to its pointed end had a T_m of 67.2 ± 0.1 °C, and actin with GS1 bound to its barbed end had a T_m of 69.1 ± 0.1 °C (Figure 6). The kinetics of unfolding at various temperatures were determined, and Arrhenius plots were constructed to determine activation energies and preexponential factors for the DNase I and GS1 TMR-actin complexes.

DISCUSSION

We have shown that there is a 21% decrease in the absorbance of TMR-actin at 557 nm upon thermal unfolding. Several experiments were performed to explain the nature of this shift. A_{557} measurements of NAc-Cys-TMR showed that the decrease in TMR-actin A_{557} observed upon thermal denaturation can only be explained by an apolar shift. The 5 nm blue shift in λ_{max} upon thermal unfolding of TMR-actin is also consistent with movement to a more apolar environment, as observed with NAc-Cys-TMR. The effect of the concentration of Ca^{2+}•ATP•TMR-actin on the T_m determined by measuring changes in A_{557} was examined (data not shown). At very low concentrations of TMR-actin, where aggregation upon unfolding is believed to be minimized, the apparent T_m of TMR-actin increased slightly, consistent with the hypothesis that the A_{557} change of TMR-actin upon thermal unfolding is due to aggregation. Taken together, our data support a mechanism whereby the A_{557} of TMR-actin changes upon protein unfolding as the TMR moiety shifts to a more apolar environment within a protein aggregate.

Modifying actin with TMR is a simple procedure which has been well characterized. It has been reported that modification of actin with TMR results in a closed conformation (*24*). Although differing in magnitude, both Ca^{2+} and Mg^{2+} TMR-actin were found to have decreased nucleotide

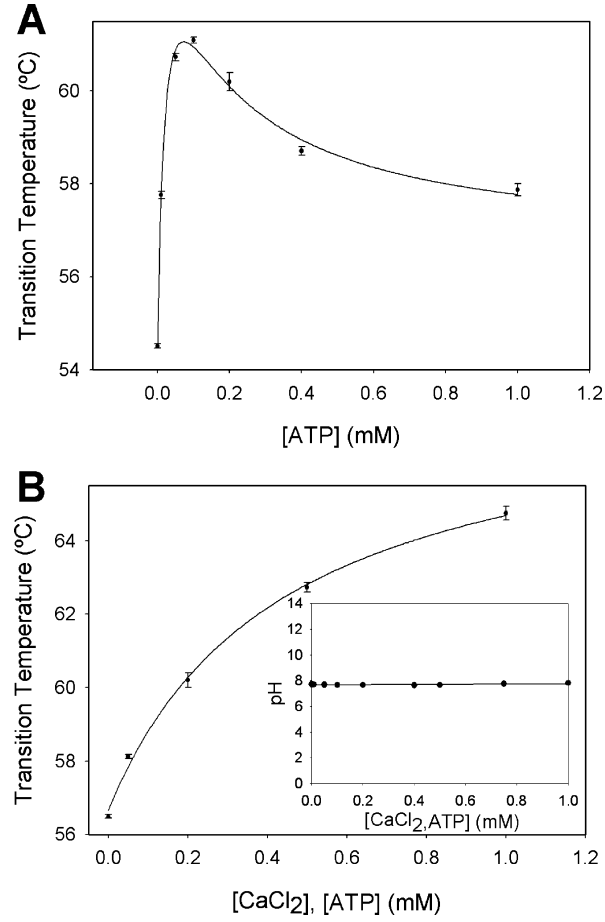

FIGURE 5: Nucleotide and cation concentrations affect the T_m of TMR-actin. (A) Varying the ATP concentration and maintaining a $CaCl_2$ concentration of 0.2 mM showed a rapid increase in T_m of Ca^{2+}•ATP-TMR-actin up to a concentration of 0.1 mM ATP. At concentrations of ATP greater than 0.1 mM the T_m was found to decrease. The data points shown for concentrations of 0, 0.01, 0.05, 0.1, 0.2, 0.4, and 1.0 mM ATP were averaged from n of 4, 5, 5, 5, 12, 5, and 3 trials, respectively. Error bars are representative of standard error. (B) Maintaining equimolar concentrations of $CaCl_2$ and ATP while increasing the total concentration exhibited an increasing trend in the T_m of Ca^{2+}•ATP-TMR-actin. Data points for 0.0, 0.05, 0.2, 0.5, and 1 mM ATP and $CaCl_2$ are averages of 6, 3, 12, 5, and 3 replicates, respectively. Error bars are representative of standard error. No significant change in pH was observed over the range of ATP and $CaCl_2$ concentrations employed (inset).

exchange rates compared to unmodified actin (*18*). Our results for Mg^{2+} and Ca^{2+} TMR-actin were similar to those previously described by Schuler et al. for unmodified actin (*7*), suggesting that chemical modification at Cys^{374} with TMR-maleimide does not affect the thermal stability of the actin monomer. In addition, previous reports show no significant difference in stability between Ca^{2+}•ATP•TMR-actin and Ca^{2+}•ATP-actin (*15*). Given the relationship between nucleotide loss and actin unfolding, our data suggest that the inhibition of nucleotide exchange by TMR-actin is lost at higher temperatures and therefore does not affect thermal unfolding of the actin monomer. This phenomenon could be a result of the movement of the highly mobile C-terminal TMR-bound end (*20*) out of the hydrophobic cleft. Such a movement could explain the slight decrease in absorbance in the initial stages of the absorbance profile; however, it is also possible that a small proportion of actin unfolds at lower temperatures.

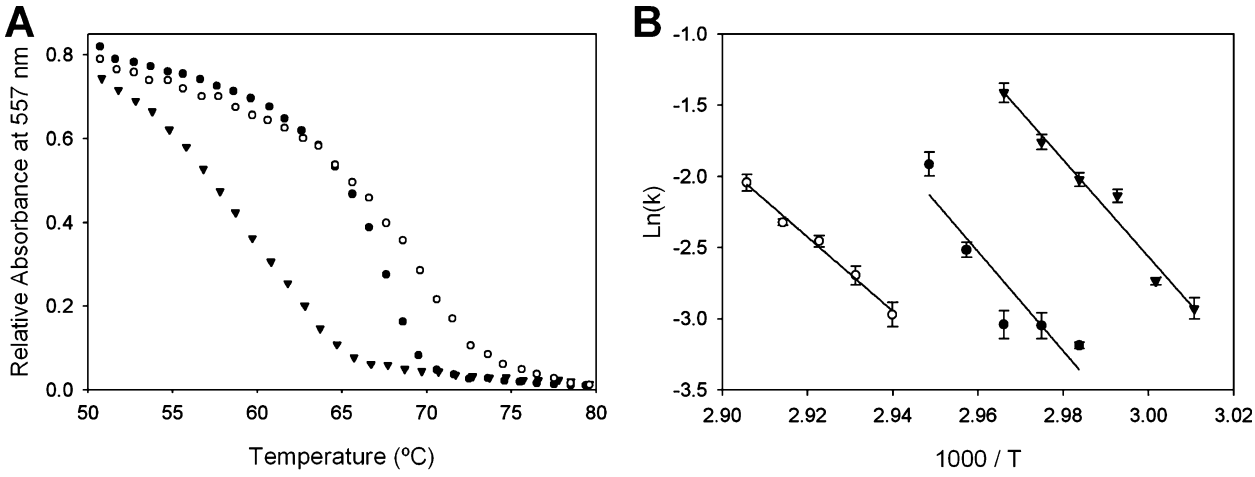

Bound Protein	$T_m \pm$ SE (°C)	E_a	ln(A)
▼ ------	60.2 ± 0.2	283 ± 24 kJ/mol[a] ; 232 ± 20 kJ/mol[b]	99[a]; 72[b]
● DNase I	67.2 ± 0.1	290 ± 95 kJ/mol	101
○ GS1	69.1 ± 0.1	216 ± 13 kJ/mol	74

[a] E_a determined from the kinetics of unfolding.
[b] E_a determined from the T_m dependence on the scan rate.

FIGURE 6: DNase I-bound TMR-actin and GS1-bound TMR-actin complexes exhibit elevated melting temperatures. (A) Purified complexes (10 μM) of Ca^{2+}•ATP-TMR-actin (closed triangle) bound by DNase I (closed circles) or GS1 (open circles) at 1:1 stoichiometries were subjected to a thermal gradient of 0.5 °C/min while the change in absorbance of TMR was monitored at 557 nm. The T_m for DNase I-bound TMR-actin was 67.2 ± 0.1 °C ($n = 3$), while the T_m for GS1-bound TMR-actin was 69.1 ± 0.1 °C ($n = 3$). The T_m was calculated as an average of triplicate assays. (B) Ca^{2+}•ATP•TMR-actin in complex with DNase I (10 μM) was subjected to temperatures of 62, 63, 64, 65, and 66 °C. Raw absorbance measurements were normalized to unity, and the rates were determined from single exponential decay curves using SigmaPlot 10 (data not shown) as in Figure 3B. The rates were plotted and fit to the Arrhenius equation to extract activation energies. The calculated E_a for the TMR-actin DNase I complex was 290 ± 95 kJ/mol with a frequency factor of 101 ± 26. Similarly, Ca^{2+}•ATP•TMR-actin in complex with GS1 (10 μM) was subjected to temperatures of 67, 68, 69, 70, and 71 °C, and the calculated E_a for the TMR-actin GS1 complex was 216 ± 13 kJ/mol with a frequency factor of 74 ± 5. All kinetic parameters were determined from data sets with $n \geq 3$.

We have shown that the measured T_m of TMR-actin depends on the thermal scan rate, confirming the irreversible nature of actin unfolding. It is important to note that although we have treated the unfolding reaction in its simplest form, MNA → I_{15}, the Sanchez-Ruiz law still applies to more complex pathways, such as MNA ⇔ A → I_{15}. Under the assumption of fast unfolding kinetics, as is the case during thermal unfolding, this pathway is equivalent to pathway 3. Additionally, the thermal scan rate must be considered when comparing T_m values between previous studies (Table 1). Our thermal scan rate data and unfolding kinetic data were used to independently determine the activation energy and preexponential factor of the unfolding reaction. The values were similar to those found in literature, emphasizing the validity and versatility of our method.

The T_m of TMR-actin with different cations and nucleotides bound follows the same trend as those for unlabeled actin measured with the DNase I inhibition assay (Ca^{2+}•ATP > Mg^{2+}•ATP > Ca^{2+}•ADP > Mg^{2+}•ADP, Table 1) (*7*). The differences in stability between the various metal−cation actin complexes are partially explained by the two-pathway model; however, a quantitative analysis is beyond the scope of the work presented here. In short, it is critical to consider actin's binding affinities for nucleotides and cations and the ratio of unfolding through either pathway 1 or 2. Furthermore, consideration of the differing free cation concentrations in solution should be given due to the varying ability of ATP and ADP to chelate free metals in solution. Using our method for actin stability determinations, a set of constant temperature experiments could be designed to quantitatively describe the effects of cations and nucleotides on actin.

It has been shown that an increase in the concentration of free calcium results in a decrease in the nucleotide exchange rate of TMR-actin (*18*), demonstrating that the dependence of the nucleotide release rate on the concentration of free cation remains true for TMR-actin. Both pathway 1 and pathway 2 are significant contributors to nucleotide loss, with pathway 1 predominating for calcium-bound actin and both pathways participating for magnesium-bound ATP actin (*25*). The two phases of Ca^{2+}•ATP-TMR-actin T_m measured with our A_{557} assay at increasing concentrations of ATP and 0.2 mM calcium (Figure 5A) can be explained with the two-pathway model. Metal loss is a prerequisite for nucleotide loss in pathway 1, and therefore unfolding through pathway 1 is governed by the concentration of calcium in solution. At concentrations of ATP below 0.1 mM, calcium is present in high concentrations and the binding of high amounts of calcium to nucleotide-bound actin increases the measured stability of the protein. In addition, unfolding occurring through the pathway 2 mechanism is increased due to the lack of high amounts of metal-coordinated ATP in solution. As the concentration of ATP increases to moderate levels, flux through pathway 1 remains low because calcium remains abundant, while flux through pathway 2 decreases due to higher Ca^{2+}•ATP concentrations in solution. As a result, the T_m of actin increases. At a threshold concentration of ATP, the free calcium concentration decreases due to the formation of Ca^{2+}•ATP and pathway 1 becomes the major unfolding pathway because the rate of nucleotide release is increased

in low calcium solutions, resulting in lower T_m values at higher ATP concentrations. An interesting observation is that maximum stability of actin appears to be acquired with about 0.1 mM ATP in buffers that contain 0.2 mM calcium, not 0.2 mM ATP as found in the traditional G-buffer for actin (*21*).

It is important to note that pathway 3 deviates slightly from the unfolding pathway described by Povarova et al. (*9*) in that the transition from MNA to A is considered reversible in our model. This is likely due to our interpretation of the nature of the intermediate, A. We have considered this intermediate to be a properly folded actin monomer lacking bound nucleotide and cation. Furthermore, we have considered this portion of the pathway to be reversible due to the nucleotide and cation dependencies discussed above. Our experimental results support reversibility of this step (MNA ⇔ A); however, they also do not preclude the existence of an irreversible intermediate preceding the partially unfolded state (MNA ⇔ A → X → U*). As Povorova et al. point out, currently there is little knowledge available describing the properties of the state(s) preceding U*.

An advantage of measuring the absorbance of TMR-actin is that it reports on the status of the actin protein in actin-containing complexes. Other techniques will typically have complex spectral results reporting on the protein complex as a whole. DNase I inhibition assays may be able to report on the state of actin in complexes, so long as the binding of another molecule to actin does not perturb the DNase I binding loop or sterically inhibit DNase I binding. Using TMR-actin absorbance, we were able to determine an increase in T_m of 7.2 °C upon binding of DNase I to TMR-actin. The same limitations apply to TMR-modified actin complexes; modification of Cys^{374} with *N*-ethylmaleimide has been shown to drastically reduce the binding affinity of profilin, and it is possible that rhodamine labeling has a similar affect on some barbed end binding proteins (*19, 26, 27*). We have determined both melting temperatures and activation energies for the complexes formed. An increase in the thermal stability of TMR-actin while complexed is indicative of an apparent stabilizing effect due to the binding proteins; however, further interpretation of the data quickly becomes complicated. First, the unfolding pathways for actin complexes are unknown: Is it a decrease in the nucleotide exchange rate that stabilizes the actin? Both DNase I and GS1 have been found to significantly reduce the rate of nucleotide exchange of actin (*22, 28*). It is likely that, in addition to adding stability to the actin monomer through protein−protein interactions, there is an added stability effect by decreasing nucleotide exchange. Second, does the complex unfold as a complex or do the proteins dissociate from each other prior to unfolding? Native PAGE analysis shows a gradual disappearance of the native complexes with an increased time at high temperatures (data not shown); however, one cannot infer whether a heterogeneous or a monodispersed aggregate is formed similar to the unfolding of uncomplexed actin.

Under physiological conditions actin possesses the ability to form long filaments. After monomers of actin come together to form filament nuclei, polymerization occurs from both ends of the nuclei to form long filaments. Many proteins bind actin or actin filaments, promoting nucleation, inducing polymerization, bundling, or cross-bridging, while other proteins possess capping, severing, or sequestering properties and inhibit filament growth. Does the stabilizing effect of these actin binding proteins contribute to the inhibition of polymerization or is it strictly a steric mechanism? Stable calcium bound G-actin does not polymerize as readily as its more unstable, magnesium-bound counterpart. Also, it has been shown that nucleotide free actin, considered unstable, possesses a critical concentration of filament formation close to zero (*5*). Thermal studies using cofilin bound G- and F-actin have provided similar inferences (*17*). While steric mechanisms are likely a dominant factor in the inhibition of polymer formation, studying the effect of binding proteins on the kinetics of free-end polymerization and correlating the data with changing actin protein stability may shed light on the regulation of filament dynamics *in vivo*.

We have shown that the decrease in absorbance at 557 nm of TMR-actin upon thermal unfolding is due to an increase in the apolarity of the environment experienced by the TMR moiety and that this is most likely due to the aggregation of unfolded actin proteins. The fact that our measurements of actin T_m and activation energies are so similar to measurements obtained by other techniques demonstrates that the unfolding of actin is limited by the loss of nucleotide and supports treatment of the unfolding reaction as a pseudo-first-order two-state irreversible reaction. Furthermore, corroboration with other work validates the technique as a method for the continuous monitoring of the thermal unfolding of TMR-actin. Our data also support the two-pathway model for actin unfolding and show that pathway 2 predominates at low ATP concentrations when calcium concentration is high and that pathway 1 predominates when the converse is true. Our results suggest a tight relationship between the two pathways with respect to nucleotide and cation concentrations. It must be stressed that a change in one pathway will likely affect the other pathway and thus complicate interpretations in trends. We also demonstrate that our A_{557} assay can be used to measure the effect of ABPs on actin stability. In summary, monitoring changes in the absorbance of TMR-actin at 557 nm is a valid means of reporting on the folding status of the actin and can be used for several studies of actin structure and function.

REFERENCES

1. Boldogh, I. R., and Pon, L. A. (2006) Interactions of mitochondria with the actin cytoskeleton. *Biochim. Biophys. Acta 1763*, 450–462.
2. Maughan, D. W. (2005) Kinetics and energetics of the crossbridge cycle. *Heart Fail. Rev. 10*, 175–185.
3. Vang, S., Corydon, T. J., Borglum, A. D., Scott, M. D., Frydman, J., Mogensen, J., Gregersen, N., and Bross, P. (2005) Actin mutations in hypertrophic and dilated cardiomyopathy cause inefficient protein folding and perturbed filament formation. *FEBS J. 272*, 2037–2049.
4. Schuler, H. (2001) ATPase activity and conformational changes in the regulation of actin. *Biochim. Biophys. Acta 1549*, 137–147.
5. De La Cruz, E. M., Mandinova, A., Steinmetz, M. O., Stoffler, D., Aebi, U., and Pollard, T. D. (2000) Polymerization and structure of nucleotide-free actin filaments. *J. Mol. Biol. 295*, 517–526.
6. Kinosian, H. J., Selden, L. A., Estes, J. E., and Gershman, L. C. (1993) Nucleotide binding to actin. Cation dependence of nucleotide dissociation and exchange rates. *J. Biol. Chem. 268*, 8683–8691.
7. Schuler, H., Lindberg, U., Schutt, C. E., and Karlsson, R. (2000) Thermal unfolding of G-actin monitored with the DNase I-inhibition assay stabilities of actin isoforms. *Eur. J. Biochem. 267*, 476–486.

8. Altschuler, G. M., Klug, D. R., and Willison, K. R. (2005) Unfolding energetics of G-alpha-actin: a discrete intermediate can be re-folded to the native state by CCT. *J. Mol. Biol. 353*, 385–396.
9. Povarova, O. I., Kuznetsova, I. M., and Turoverov, K. K. (2007) Different disturbances-one pathway of protein unfolding. Actin folding-unfolding and misfolding. *Cell Biol. Int. 31*, 405–412.
10. Kuznetsova, I. M., Biktashev, A. G., Khaitlina, S. Y., Vassilenko, K. S., Turoverov, K. K., and Uversky, V. N. (1999) Effect of self-association on the structural organization of partially folded proteins: inactivated actin. *Biophys. J. 77*, 2788–2800.
11. Le, B. T., and Gicquaud, C. (1993) Kinetic study of the thermal denaturation of G actin using differential scanning calorimetry and intrinsic fluorescence spectroscopy. *Biochem. Biophys. Res. Commun. 194*, 1065–1073.
12. Contaxis, C. C., Bigelow, C. C., and Zarkadas, C. G. (1977) The thermal denaturation of bovine cardiac G-actin. *Can. J. Biochem. 55*, 325–331.
13. Bertazzon, A., Tian, G. H., Lamblin, A., and Tsong, T. Y. (1990) Enthalpic and entropic contributions to actin stability: calorimetry, circular dichroism, and fluorescence study and effects of calcium. *Biochemistry 29*, 291–298.
14. Bookwalter, C. S., and Trybus, K. M. (2006) Functional consequences of a mutation in an expressed human alpha-cardiac actin at a site implicated in familial hypertrophic cardiomyopathy. *J. Biol. Chem. 281*, 16777–16784.
15. Kudryashov, D. S., Phillips, M., and Reisler, E. (2004) Formation and destabilization of actin filaments with tetramethylrhodamine-modified actin. *Biophys. J. 87*, 1136–1145.
16. Mikhailova, V. V., Kurganov, B. I., Pivovarova, A. V., and Levitsky, D. I. (2006) Dissociative mechanism of F-actin thermal denaturation. *Biochemistry (Moscow) 71*, 1261–1269.
17. Dedova, I. V., Nikolaeva, O. P., Mikhailova, V. V., dos Remedios, C. G., and Levitsky, D. I. (2004) Two opposite effects of cofilin on the thermal unfolding of F-actin: a differential scanning calorimetric study. *Biophys. Chem. 110*, 119–128.
18. Kudryashov, D. S., and Reisler, E. (2003) Solution properties of tetramethylrhodamine-modified G-actin. *Biophys. J. 85*, 2466–2475.
19. Pelikan, C. A., Didry, D., Le, K. H., Larquet, E., Boisset, N., Pantaloni, D., and Carlier, M. F. (2006) Analysis of tetramethylrhodamine-labeled actin polymerization and interaction with actin regulatory proteins. *J. Biol. Chem. 281*, 24036–24047.
20. Otterbein, L. R., Graceffa, P., and Dominguez, R. (2001) The crystal structure of uncomplexed actin in the ADP state. *Science 293*, 708–711.
21. Spudich, J. A., and Watt, S. (1971) The regulation of rabbit skeletal muscle contraction. I. Biochemical studies of the interaction of the tropomyosin-troponin complex with actin and the proteolytic fragments of myosin. *J. Biol. Chem. 246*, 4866–4871.
22. Dawson, J. F., Sablin, E. P., Spudich, J. A., and Fletterick, R. J. (2003) Structure of an F-actin trimer disrupted by gelsolin and implications for the mechanism of severing. *J. Biol. Chem. 278*, 1229–1238.
23. Sanchez-Ruiz, J. M., Lopez-Lacomba, J. L., Cortijo, M., and Mateo, P. L. (1988) Differential scanning calorimetry of the irreversible thermal denaturation of thermolysin. *Biochemistry 27*, 1648–1652.
24. Sablin, E. P., Dawson, J. F., VanLoock, M. S., Spudich, J. A., Egelman, E. H., and Fletterick, R. J. (2002) How does ATP hydrolysis control actin's associations? *Proc. Natl. Acad. Sci. U.S.A. 99*, 10945–10947.
25. Valentin-Ranc, C., and Carlier, M. F. (1989) Evidence for the direct interaction between tightly bound divalent metal ion and ATP on actin. Binding of the lambda isomers of beta gamma-bidentate CrATP to actin. *J. Biol. Chem. 264*, 20871–20880.
26. Plank, L., and Ware, B. R. (1987) Acanthamoeba profilin binding to fluorescein-labeled actins. *Biophys. J. 51*, 985–988.
27. Malm, B. (1984) Chemical modification of Cys-374 of actin interferes with the formation of the profilactin complex. *FEBS Lett. 173*, 399–402.
28. Hitchcock, S. E. (1980) Actin deoxyroboncuclease I interaction. Depolymerization and nucleotide exchange. *J. Biol. Chem. 255*, 5668–5673.

BI800421U